Dynamic Article Links ►

Cite this: DOI: 10.1039/c0xx00000x

www.rsc.org/xxxxxx

ARTICLE TYPE

Active Guests in MoS_2 / $MoSe_2$ Host Lattice: Efficient Hydrogen Evolution Using Few-Layer Alloys of $MoS_{2(1-x)}Se_{2x}$

Vankayala Kiran, Debdyuti Mukherjee, Ramesh Naidu Jenjeti and Srinivasan Sampath*

Received (in XXX, XXX) Xth XXXXXXXXX 20XX, Accepted Xth XXXXXXXXX 20XX

DOI: 10.1039/b000000x

Few layer transition metal dichalcogenide alloys based on molybdenum sulphoselenides [$MoS_{2(1-x)}Se_{2x}$] possess higher hydrogen evolution (HER) activity as against pristine few layer MoS_2 and $MoSe_2$. Variation of sulphur or selenium content in the parent dichalcogenides reveals a systematic structure-activity relationship for different compositions of alloys and it is found that the composition, $MoS_{1.0}Se_{1.0}$, possesses the highest HER activity amongst the catalysts studied. Tunable electronic structure of MoS_2/$MoSe_2$ upon Se/S incorporation probably assists in the realization of high HER activity.

Two-dimensional (2D) layered materials have been very fascinating in terms of electronic and electrochemical properties.[1,2] They possess weak van der Waals forces between molecular layers and strong chemical bonding within the layers. The exfoliation of 2D materials into thin sheets has led to interesting properties that have attracted enormous attention.[3-7] Various strategies have been proposed to realize the inorganic analogues of graphene based on layered dichalcogenides.[3-7] It has been shown that the physical and chemical properties of 2D materials such as MoS_2, WS_2, $MoSe_2$ and WSe_2 can be tuned by thinning the material into their ultimate dimension of a single layer.[8-10] For instance, bulk MoS_2 which is an indirect band gap semiconductor becomes a direct band gap semiconductor when it is exfoliated to a single layer.[9,10] The versatility of these materials can be further enhanced by engineering the layered materials, by several ways such as constructing heterostructures or by chemical doping.[11-20] Recently, various experimental and theoretical efforts have been dedicated to study properties of transition metal dichalcogenide alloys such as $Mo_{1-x}W_xS_2$ and $MoS_{2(1-x)}Se_{2x}$.[14-18,21,22] A change in electronic structure has been noticed upon incorporation of species like W in MoS_2, Se in MoS_2 etc.[14-18] It has been reported that a systematic variation of properties can be realized by tuning the composition of the dichalcogenide alloys. For example, the band gap photoluminescence of $MoS_{2(1-x)}Se_{2x}$ systems, can be continuously varied between 1.87 eV (single-layer MoS_2) and 1.55 eV (single layer$MoSe_2$) by tuning the composition.[18]

The development of 2D materials towards various applications in photodetectors, batteries, field effect transistors, photocatalysis, electrocatalysis etc. has been a very active area of research in recent years.[2] In particular, the electrocatalytic activity of few layer MoS_2 and other transition metal dichalcogenides (TMD) has received considerable attention.[21-23] Various TMDs have been proposed as efficient non-Pt catalysts for HER, including a recent report on layered-like PdPS from our group.[21-29] The free energy of hydrogen adsorption (ΔG_H^o) is found to be close to thermo-neutrality for MoS_2 and makes it an efficient HER catalyst.[21,22] The electroactivity of TMDs can be tuned by altering their electronic structure[23] and there have been recent efforts to enhance the HER activity on TMD.[28-33] For example, high HER activities are achieved for 1T polytype phase of MoS_2/WS_2[29,30] as compared to that on 2H phase. Cui et al. have reported a methodology based on electrochemical intercalation to tune the activity of MoS_2, wherein insight into multiple properties such as oxidation state tunability of Mo, the transition of semiconducting 2H to metallic 1T phase, and their effect on HER have been studied.[5] The HER activity of MoS_2 has been shown to be improved by the presence of Se, Co, Fe or Ni.[34,35] The present study aims at the use of alloys of the type $MoS_{2(1-x)}Se_{2x}$ for efficient electrocatalysis of HER. Tunable HER activities have been observed and a notable dependence of S/Se ratio on HER activity has been identified. The alloys are found to be better than the parent compounds and the highest catalytic activity is achieved for the $MoS_{1.0}Se_{1.0}$ phase.

Molybdenum sulphoselenides are prepared using high temperature solid state reaction technique. Typically, $MoS_{2(1-x)}Se_{2x}$ crystals are obtained by heating the mixture of constituent elements in the required atomic ratio in evacuated quartz tube at 800°C for 3 days. The as-obtained crystals are characterized for phase and purity using various techniques. X-ray diffraction (XRD) patterns and the variation of lattice parameter of $MoS_{2(1-x)}Se_{2x}$ are shown in figures S1 & S2 and the data indicate that the samples are highly crystalline and the reflections for $MoS_{1.0}Se_{1.0}$ match well with reported patterns (JCPDF No 36-1408). The details are given in supporting information. The crystals are further examined using Raman spectroscopy. As shown in figure S3, (†ESI) the Raman spectrum of $MoS_{2(1-x)}Se_{2x}$ consists of bands in low wave number region (100-500 cm^{-1}) and can be divided into two parts, one part is MoS_2-like and another is $MoSe_2$-like bands. The bands around 371 cm^{-1} and 400 cm^{-1} are due to MoS_2-like and are attributed to E_{2g} (in-plane) and A_{1g} (out-of-plane) modes respectively.[4] Similarly, the second part "$MoSe_2$-like" consists of bands around 224 and 264 cm^{-1}, slightly shifted to lower wave number values than that of pure $MoSe_2$.[25] These bands are attributed to A_{1g} and E_{2g} modes. Apart from these two

Cite this: DOI: 10.1039/c0xx00000x

www.rsc.org/xxxxxx

ARTICLE TYPE

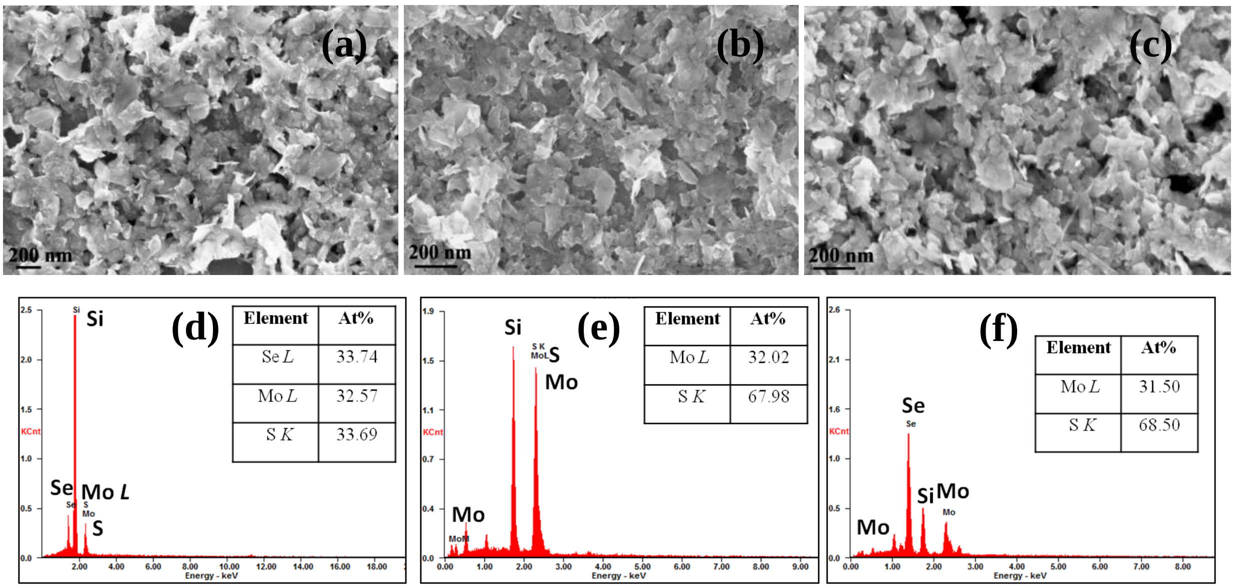

Figure 1. FESEM images of few layer (a) $MoS_{1.0}Se_{1.0}$, (b) MoS_2 and (c) $MoSe_2$ nanosheets and (d) to (f) corresponding EDS data.

groups of bands, the spectra reveal the presence of new bands around 355 and 260 cm^{-1}, whose positions are also sensitive to the composition. It is believed that the bands are due to the so-called two-mode behaviour as reported earlier for similar systems, for example $CdS_xSe_{(1-x)}$.[36,37] It is quite reasonable to assign these bands to two-mode behaviour as the frequencies of phonon modes corresponding to pure MoS_2 and $MoSe_2$ are sufficiently well separated from each other. In the case of the alloy composition, $Mo_{1-x}W_xS_2$, the difference between phonon frequencies is ~ 50 cm^{-1}. The origin of these bands is still unclear and requires further investigation. As shown in figure S3, the intensities of MoS_2-like bands for $MoS_{2(1-x)}Se_{2x}$ decrease with increase in Se composition along with shifts towards lower frequencies. In other words, MoS_2/$MoSe_2$ - like bands soften upon Se/S incorporation [figure S3 (b)]. It is also possible that the shift and split of Raman bands are due to the residual strain offered by selenium incorporation in MoS_2 or vice versa. Extensive Raman spectroscopic analysis on these aspects will be reported elsewhere.

Field emission scanning electron microscopic (FESEM) images of bulk $MoS_{1.0}Se_{1.0}$ crystals consist of platelet-like morphology [Figure S4(a)] and the energy dispersive X-ray analysis (EDS) data indicate the presence of ~1:1 atomic percentage of S and Se (Figure S4, † ESI). Other compositions of selenium- or sulphur- rich sulphoselenides show similar behaviour.

The bulk crystals are exfoliated into few layer sulphoselenide nanosheets by adopting a procedure reported earlier for various TMDs such as MoS_2 and WS_2.[6] A mixed solvent methodology is used to prepare few layer $MoS_{1.0}Se_{1.0}$ nanosheets and the details are given in supporting information. Figure 1(a) shows the FESEM image of few layer $MoS_{1.0}Se_{1.0}$ nanosheets which reveals the presence of ultrathin sheet-like morphology with lateral dimensions of around 100 - 300 nm. The presence of ripples and corrugations are found to be similar to other 2D nanostructures such as graphene and MoS_2.[7] As evident from figure 1, no detectable difference in terms of morphology has been noted for the MoS_2 and $MoSe_2$ nanosheets. Further, EDS data indicate the presence of S along with Se in the case of few layers of $MoS_{1.0}Se_{1.0}$ with ~1:1 atomic percentage of S and Se, as that observed for bulk crystals. It is noteworthy that the material retains its composition after exfoliation, without any appreciable change in the composition.

The thickness of the nanosheets as measured using atomic force microscopy (AFM) in the tapping mode is shown in figure 2. The thickness of $MoS_{1.0}Se_{1.0}$ nanosheets fall in the range of 1.4-1.9 nm, suggesting that the sample consists of few layers. It is worth noting that single layers of $MoS_{1.0}Se_{1.0}$ are also observed in certain places where the thickness is found to be 0.6-0.8 nm. Also, the thickness of pristine MoS_2 and $MoSe_2$ are comparable to that of $MoS_{1.0}Se_{1.0}$, $MoSe_2$ being slightly higher than others. The 3D version of figure is shown in supporting information (figure S5). The dispersions are further examined using dynamic light scattering technique. The data (Table S1, †ESI) indicate hydrodynamic sizes in the range 125 ± 20 nm for all the compositions. All these observations suggest that the alloys and pristine materials possess similar dimensions, especially the thickness. The aqueous dispersions of the nanostructures are highly stable and typical photograph of the colloids show Tyndall light scattering effect (Figure S6, †ESI), which is an indication of

Cite this: DOI: 10.1039/c0xx00000x

www.rsc.org/xxxxxx

ARTICLE TYPE

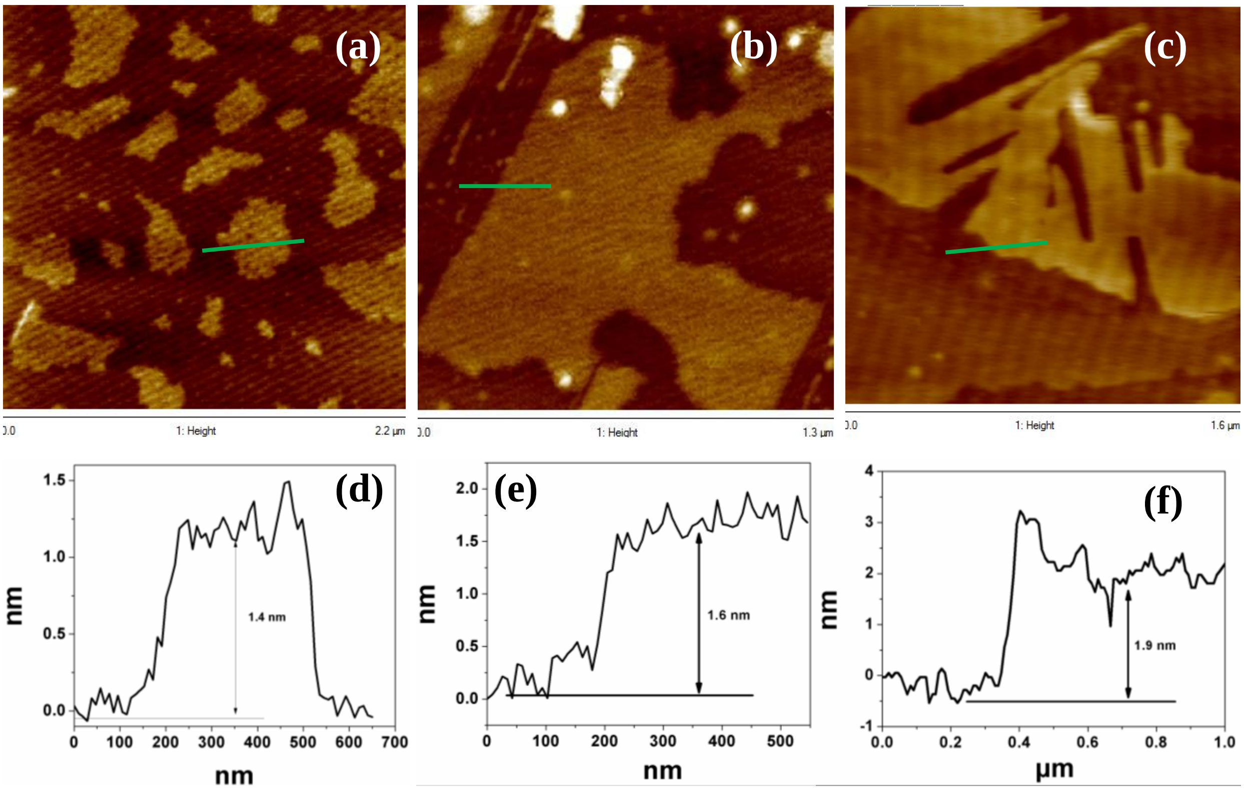

Figure 2. AFM images of few layer (a) $MoS_{1.0}Se_{1.0}$, (b) MoS_2 and (c) $MoSe_2$ nanosheets and (d) to (f) corresponding height profiles from the regions marked in the figure. Figures a,b and c are scanned in the range 0-2.2 µm; 0-1.3 µm and 0-1.6 µm respectively.

the presence of exfoliated layers in aqueous dispersions. Optical properties of few layer $MoS_{2(1-x)}Se_{2x}$ colloidal dispersions are determined using various spectroscopic tools. Figure 3a and 3b shows UV-Vis absorbance data corresponding to few layer $MoS_{2(1-x)}Se_{2x}$ with varying values of x. The data represents the presence of two prominent peaks. The peak located at high wavelength is generally termed as exciton A and the one at lower wavelength is exciton B.[38] The origin of these peaks is from the direct excitonic electronic transition at K point of the first Brillouin zone.[38,10] The origin of energy difference between excitons A and B is due to spin-orbit coupling of valence band. Figure 3(b) shows the energy difference between excitons A and B along with their absolute values as a function of Se content. As shown in the figure, the peaks shift monotonically towards lower energies with Se content. The energy difference between peaks A and B vary linearly with Se content. This infers that the bowing parameters of exciton A and exciton B are close to each other. The valence band spin-orbit coupling changes from 0.18 to 0.25 with increase in Se content. The spectra shown in the present study correlates well with the theoretical studies.[39]

X-ray photoelectron spectroscopy (XPS) analysis [Figures 3(c) and 3(d)] of few layer $MoS_{2(1-x)}Se_{2x}$ shows the presence of all the constituents. As shown in figure 3(c), two peaks corresponding to Mo-$3d_{5/2}$ and Mo-$3d_{3/2}$ levels are observed. Similar peak positions for MoS_2 and $MoSe_2$–based systems have been reported earlier.[5,21] It is noteworthy that the peaks corresponding to alloys shift to low binding energy (B.E) values (Mo-3d, 228.9 eV and 232.1 eV) as compared to MoS_2 (229.4 eV and 232.6 eV). Further, as shown in figure 3(c), the Mo-3d spectra corresponding to MoS_2 and $MoS_{1.0}Se_{1.0}$ exhibit a peak around 226.7 eV and is due to S-2s, which is absent in the case of $MoSe_2$. Also, as shown in figure 3(d), it is observed that with increasing value of x, the intensity of peaks due to S-2p (located at 162.4 eV for $2p_{3/2}$ and at 163.6 eV for $2p_{1/2}$) decreases while the peaks due to Se-$3p_{3/2}$ (at 160.4 eV) and Se-3d (at 54.5 eV) (Figure S7, †ESI) become prominent. Quantitative analysis has been performed for S and Se present in the composites (†ESI). The sulphur to selenium ratios of 1:0 (S:Se); 1.49:0.50; 0.98:1; 0.81:1.20; 0.53:1.5 and 0:1 are obtained for $MoS_{2(1-x)}Se_{2x}$ where x=0, 0.25, 0.5, 0.6, 0.75 and 1 respectively (Table S2, †ESI). A good correlation with the experimental compositions is observed, which makes the methodology very efficient to realize wide range of well-defined compositions.

Figure 4 shows the typical TEM bright field image of few layer $MoS_{1.0}Se_{1.0}$ nanosheets confirming ultra thin morphology and the EDS data shows the presence of Mo, S and Se. Figure 4(c) represents the high resolution TEM (HRTEM) image of

Cite this: DOI: 10.1039/c0xx00000x
www.rsc.org/xxxxxx

ARTICLE TYPE

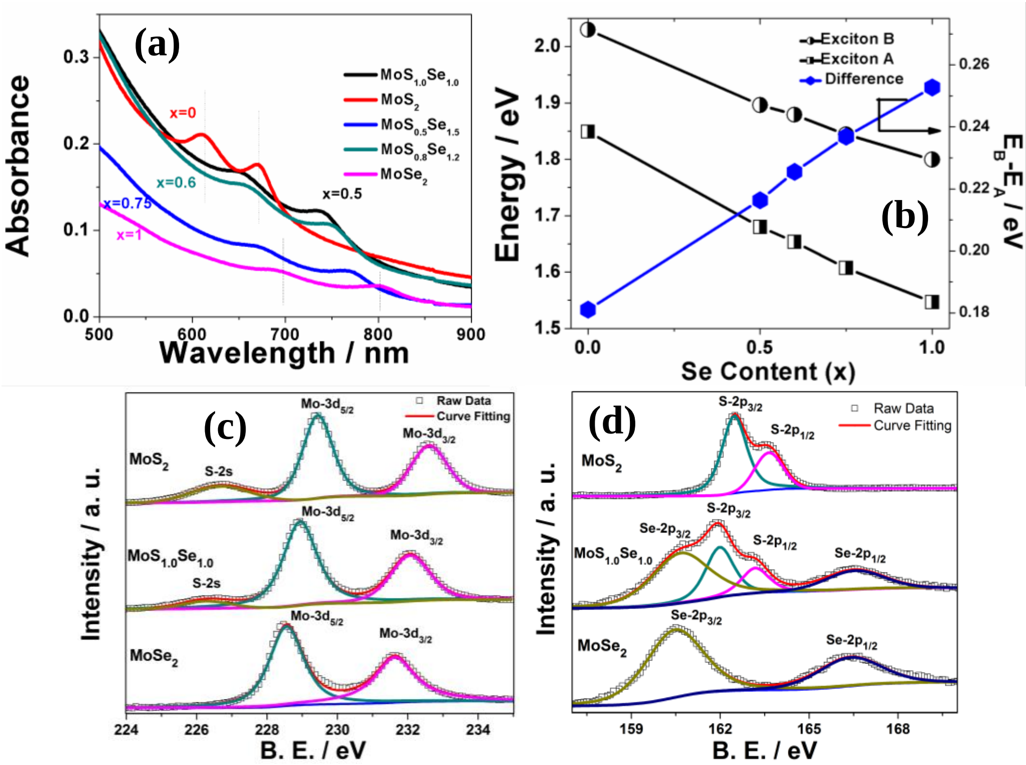

Figure 3. (a) Absorbance spectra of $MoS_{2(1-x)}Se_{2x}$ with varying x and (b) shows energies of exciton A, B and energy difference of exciton A and B as a function of Se content. (c&d) show XPS of Mo-3d and S-2p regions corresponding to $MoS_{2(1-x)}Se_{2x}$ with different x values.

$MoS_{1.0}Se_{1.0}$. Typical few layer, lamellar morphology with layer spacing of 0.65 nm is observed. The image also shows the presence of 3-4 layers of the $MoS_{1.0}Se_{1.0}$ with high crystallinity. An interplanar distance of 0.282 nm is observed (Figure 4d) and is consistent with the (100) plane of hexagonal $MoS_{1.0}Se_{1.0}$ (JCPDF No. 36-1408). Using Z-contrast TEM imaging, it has earlier been reported that Se is distributed in a random fashion in MoS_2 when Se is incorporated in MoS_2.[17] Similar observations have been put forth for $Mo_{1-x}W_xS_2$, wherein randomly distributed dopant has been observed using TEM imaging in Z-contrast mode.[40] Based on these observations, we presume that the sulphoselenide compositions of $MoS_{2(1-x)}Se_{2x}$ prepared in the current study also have S and Se present in random fashion. Figure 4(f)-4(g) represents EDS mapping of Mo, S and Se from the region shown in 4(e). The data suggests uniform and homogeneous distribution of constituents across the nanosheets.

The electrochemical activities of various compositions of few layer $MoS_{2(1-x)}Se_{2x}$ are evaluated for HER keeping the parameters such as loading of the catalyst, size of the exfoliated material and electrode area, the same. Figure 5(a) represents the iR-corrected linear sweep voltammograms recorded in N_2-saturated 0.5 M H_2SO_4 solution. The data clearly indicates the positive role of Se in MoS_2 lattice or S in $MoSe_2$ lattice towards HER. The onset potential for HER in the case of few layer $MoS_{1.0}Se_{1.0}$ is more positively shifted as compared to that of the few layer pristine MoS_2 and $MoSe_2$ nanosheets. Similar observations are made for all the other compositions of sulphoselenides. The remarkable observation is that the alloys (sulphoselenides) are always found to be better than the pure sulphides and selenides individually (Figure S8, †ESI). Among all compositions, $MoS_{1.0}Se_{1.0}$ possess high efficacy when compared to other compositions. Further, Tafel slope, a typical parameter that is used to evaluate the electroactivity and mechanism of HER, is determined from the linear region of the data shown in figure 5(c). The measurements are performed by polarizing the electrode at very slow scan rate, to eliminate mass transport effects. Typical Tafel slope obtained for MoS_2 is 96 mV dec^{-1} and for $MoSe_2$, it is 95 mV dec^{-1} while the value is around 56 mV dec^{-1} for $MoS_{1.0}Se_{1.0}$. Other alloy compositions show Tafel slopes of ~ 85 mV dec^{-1} (Table S3†, ESI). Similar Tafel slopes have been reported earlier for MoS_2-based systems.[31,32,35] The exchange current obtained from the polarization curves are 320, 45 and 36 μA cm^{-2} for $MoS_{1.0}Se_{1.0}$, $MoSe_2$ and MoS_2 respectively for a constant loading of 180 μg/cm^2. High exchange current density values portray facile HER kinetics and hence high activity. It is found that the $MoS_{1.0}Se_{1.0}$ phase possesses the highest HER activity. Further, AC impedance

Cite this: DOI: 10.1039/c0xx00000x

www.rsc.org/xxxxxx

ARTICLE TYPE

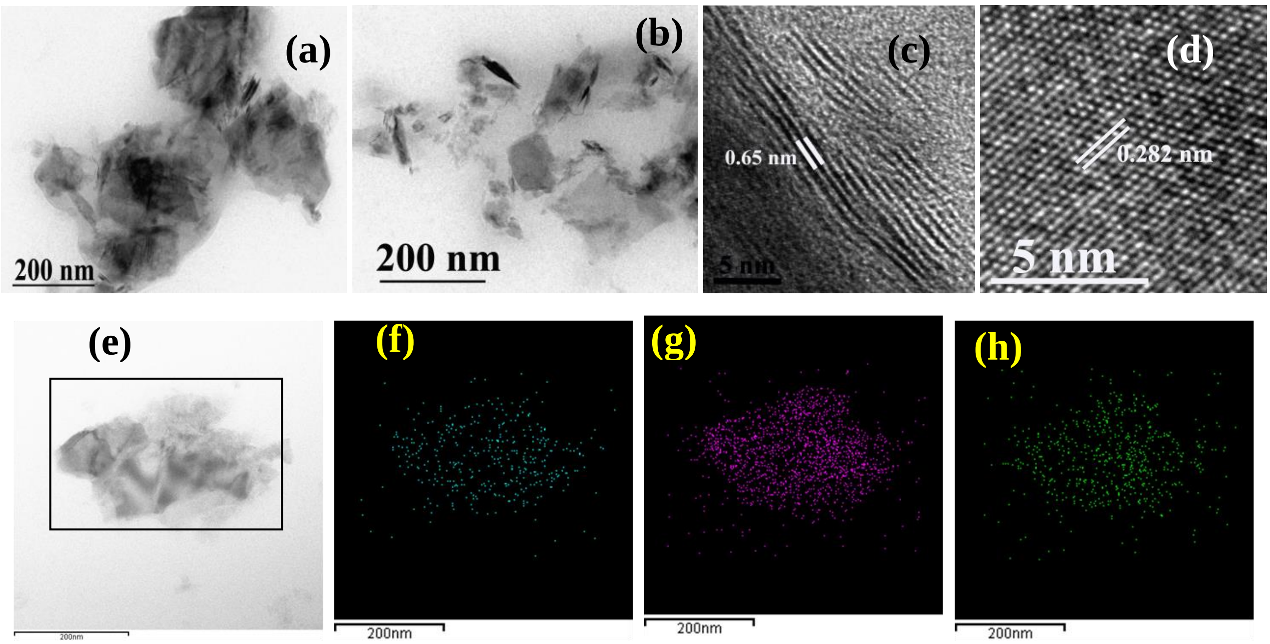

Figure 4. (a&b) TEM images of $MoS_{1.0}Se_{1.0}$ nanosheets. (c) and (d) correspond to HRTEM images of $MoS_{1.0}Se_{1.0}$. (e) STEM-BF image of MoSSe nanosheets. (f) Mo, (g) S and (h) Se mappings corresponding to the regions shown in figure (e).

measurements show charge transfer resistance (R_{CT}, obtained from the diameter of the semi- circle of Z' versus Z'' plot, figure S9†, ESI) being low for $MoS_{1.0}Se_{1.0}$ as compared to MoS_2 and $MoSe_2$. This indicates that the kinetics of HER is more facile on $MoS_{1.0}Se_{1.0}$ than that of its pristine counterparts. The R_{CT} values obtained are 0.45, 16, 18 and 0.048 kΩ at -0.13 V vs. RHE for $MoS_{1.0}Se_{1.0}$, MoS_2, $MoSe_2$ and Pt-C respectively.

As reported for MoS_2,[19,20,26] few layer $MoS_{2(1-x)}Se_{2x}$ composites are better than the corresponding bulk samples (Figure 5b and Figure S10†, ESI). It is also observed that the bulk alloys reveal better activity than the bulk pristine sulphide or selenide crystals (Figure S11†, ESI). This observation indicates that alloys possess possibly higher content of active (edge) sites, than that of MoS_2 and $MoSe_2$. Further, the obtained Tafel slopes for bulk crystals are around 120 mV dec^{-1} (Figure S12†, ESI) and are comparable with the values reported earlier.[5,28] This suggests the involvement of different HER mechanism on bulk surfaces as against few-layer samples. It has been reported earlier that HER in acidic media involves three possible reactions as given in equations (1)-(3).

$$H_3O^+ + e^- \rightarrow H_{ads} + H_2O \quad (1)$$

$$H_{ads} + H_3O^+ + e^- \rightarrow H_2 + H_2O \quad (2)$$

$$H_{ads} + H_{ads} \rightarrow H_2 \quad (3)$$

where H_{ads} indicates adsorbed hydrogen on catalytic site. Equation (1) is termed as Volmer equation and the Tafel slope for this step is found out to be 120 mV (b=2.3RT/αF), assuming the α to be 0.5. Equation (2) and (3) are known as Heyrovsky and Tafel reactions respectively. The slopes associated with each of these two processes are 40 mV [equation (2)] and 30 mV [equation (3)], respectively. It has also been reported that there can be another process after the first step [equation (1)] called 'spill-over process', wherein H_{ads}^* formed during electrochemical discharge step migrates to a site wherein H_{ads} gets stabilized on the electrode surface [equation (4)],[34] followed by the formation of H_2 either by Heyrovsky or by Tafel reaction steps. The Tafel slope for this process is reported to be around 60 mV.

$$H_{ads}^* \rightarrow H_{ads} \quad (4)$$

Accordingly based on above considerations, in the present case, Tafel slopes of around 120 mV/dec for bulk samples (Figure S12) indicates that Volmer equation is the rate determining step (RDS) whereas for few-layer samples, the RDS may involve the spillover step as the experimental Tafel slopes fall in the range of 50 - 60 mV/dec. Similar observations have been reported earlier for other systems.[34] The plausible explanation for the low Tafel slope values and high HER activity of $MoS_{1.0}Se_{1.0}$ phases may be due to improved electronic conductivity (Figure S13†, Table S4 ESI) upon Se incorporation into MoS_2 lattice as the former modifies the electronic band gap of MoS_2. Secondly, it is well-known that the free energy of hydrogen adsorption (ΔG_H^o) dictates the electroactivity of HER for a particular catalyst. Norskov et al. have suggested that the ΔG_H^o on MoS_2 surface is 0.08 eV for Mo-edge sites and 0.18 eV for S-edge sites[21,26] and -0.14 eV for $MoSe_2$[25] (for a hydrogen coverage of 75%). Additionally, a recent report shows the incorporation of Co leads to positive effect for MoS_2 towards HER.[26,35]

Cite this: DOI: 10.1039/c0xx00000x
www.rsc.org/xxxxxx

ARTICLE TYPE

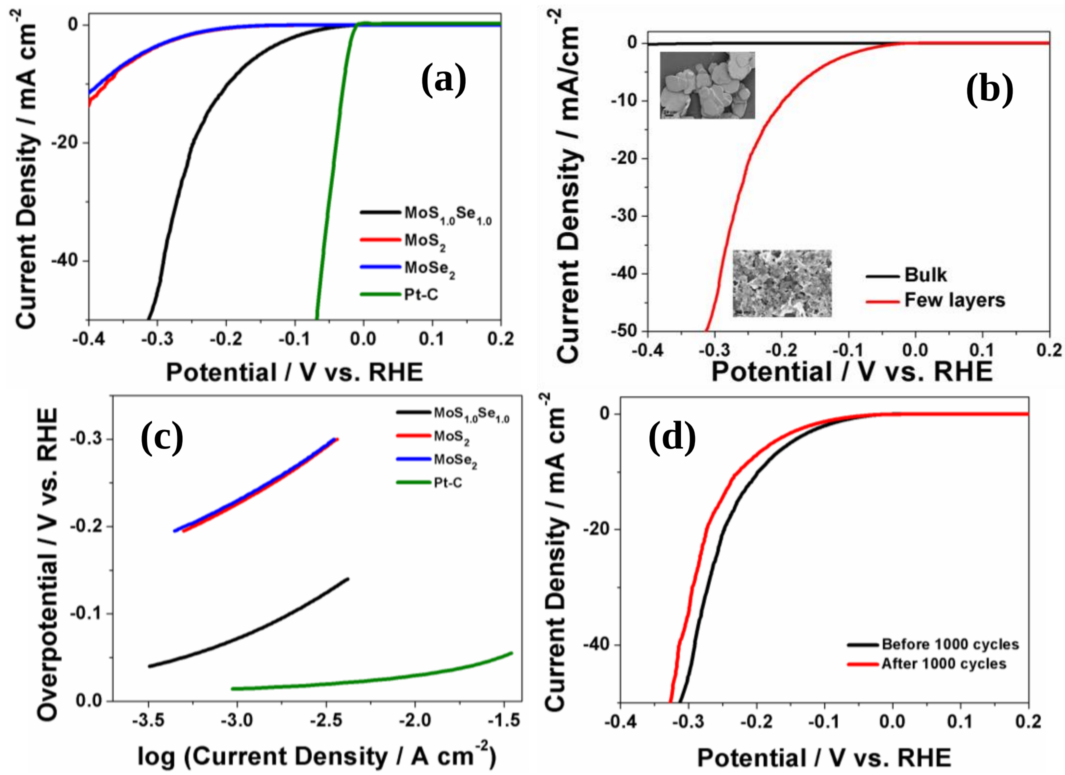

Figure 5. (a) iR-corrected linear sweep voltammograms of $MoS_{2(1-x)}Se_{2x}$ with x=0 (red), x=1 (blue), x=0.5 (black) and Pt-C (green) (b) represents voltammograms recorded on bulk and few layer $MoS_{1.0}Se_{1.0}$ nanosheets. (c) shows Tafel plots of corresponding to $MoS_{2(1-x)}Se_{2x}$ and Pt-C. (d) depicts electrochemical stability of few layer $MoS_{1.0}Se_{1.0}$ nanosheets. Electrolyte used is N_2-saturated 0.5 M H_2SO_4 and scan rate used is 1 mV/sec.

Accordingly, in the present study, it is envisaged that the presence of Se in MoS_2 lattice or S in $MoSe_2$ lattice modifies the electronic structure and thereby the ΔG_H^o as it is clearly observed that MoSSe - type phases possess higher activity than MoS_2 or $MoSe_2$. The presence of S/Se in MoS_2/$MoSe_2$ lattice may introduce defects and residual strain which can also help in improving HER activity of alloys. The presence of Se in MoS_2 lattice may induce notable strain (curvature) due to larger size of Se than sulphur. Hu et al. observed similar curvature in (002) basal planes upon Se substitution in MoS_x and claimed that the significant curvatures of (002) planes is due to the presence of selenium.[41] It is likely that similar curvature is present in the case of alloys as compared to MoS_2 where the layers are moderately straight (figure S14) and the layer-bending might induce some strain in the hexagonal lattice of alloy phases. Strain induced by local lattice distortions along with the presence of metallic phase has been shown to have positive influence on HER in the case of WS_2[29]. Similar arguments may hold for the sulphoselenides, though it is speculative at this stage. The splitting and shift in Raman bands corresponding to out of plane and in-plane vibrations of bands (MoS_2-like) points on to symmetry breaking due to strain. However, we should quickly point out that the lattice parameter varies as a function of composition (Figure S2†, ESI). This aspect requires further investigation. The surface oxidation state of Mo has also been shown to influence the HER activity.[5] As shown in figure 3(c), there is a slight shift of Mo-3d peaks to lower BE values as observed in reference 5 for MoS_2-based systems. The sulphoselenides possibly possess high active edge sites as compared to individual MoS_2 and $MoSe_2$ since the S / Se substitution is known to be random in the alloy phases. Among the alloys studied, $MoS_{1.0}Se_{1.0}$ is better than the selenium-rich or sulphur-rich compositions (Figure 6). The kinetic parameters obtained for all compositions are given in the supporting information [Figure 6(b) and Table S3†, ESI].

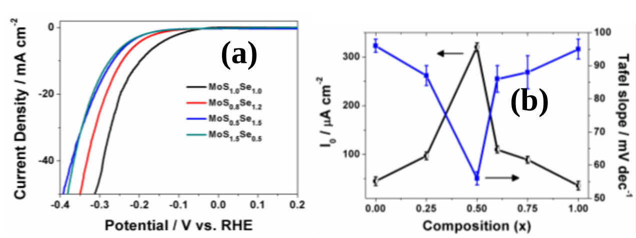

Figure 6. (a) Linear sweep voltammograms of $MoS_{2(1-x)}Se_{2x}$ with varying amounts of x. Electrolyte used is N_2-saturated 0.5 M H_2SO_4 and scan rate used is 1 mV/sec. (b) Exchange current density and Tafel slopes of the catalysts ($MoS_{2(1-x)}Se_{2x}$) studied.

High HER activity of alloys is further confirmed using Faradaic efficiency measurements with the setup shown in figure S15†, ESI. In this study, the quantity of gas evolved at the electrode surface is monitored as a function of time at constant DC bias. As shown in figure 7, the $MoS_{1.0}Se_{1.0}$ can generate higher amount of H_2 as compared to MoS_2 and $MoSe_2$ recorded under identical conditions, complementing voltammetric data as discussed earlier.

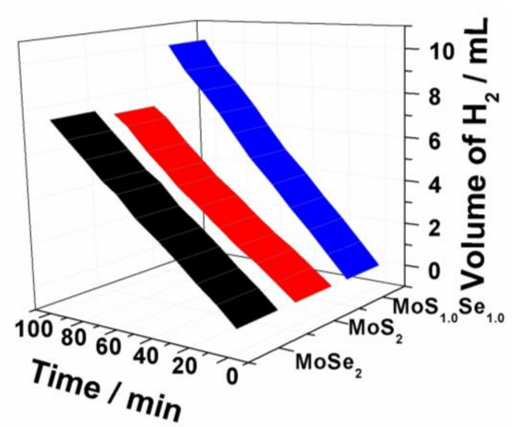

Figure 7. Quantity of H_2 evolved as a function of time at constant potential of -0.475 V vs. RHE. Electrolyte used is 0.5 M H_2SO_4.

A good correlation between experimental and theoretical efficiency indicates nearly 100% faradaic efficiency (figure S16†, ESI). The hydrogen production efficiency of $MoS_{2(1-x)}Se_{2x}$ (for example, x=0.5) is found to be superior to several reported catalysts such as MoS_3 particles, amorphous MoS_x prepared by electro-poymerization and MoS_2/reduced graphene oxide.[35,42]

Stability is one of the concerns in HER as good catalysts such as nanosized Ni-Mo[43] suffer from long term operation stability. Electrochemical cycling is performed for 1000 cycles, to understand the long term stability of sulphoselenides. As shown in figure 3(d), the voltammograms show no detectable difference between initial voltammogram and the one after 1000 cycles, indicating excellent electrochemical stability of $MoS_{1.0}Se_{1.0}$ nanosheets.

Conclusions

Thus, the present study demonstrates that the HER activity can be improved by Se substitution into MoS_2 lattice or vice versa. It opens up a way to alter the electroactivity of layered chalcogenides by fine tuning of the composition. The activity of these sulphoselenides could be further enhanced by placing them on proper supports such reduced graphene oxide, carbon paper etc. This may also have positive effects in the photocatalytic evolution of hydrogen on layered chalcogenides. These studies are being pursued.

Acknowledgements

This work is supported by DST, New Delhi. VK, RJ and DM thank CSIR for fellowship.

Notes and references

[a] *Department of Inorganic and Physical Chemistry, Indian Institute of Science, Bangalore-560012, India. Fax: +91 80 23600085; Tel: +91 80 22933315; E-mail: sampath@ipc.iisc.ernet.in*

† Electronic Supplementary Information (ESI) available: Experimental details of synthesis and characterization of $MoS_{2(1-x)}Se_{2x}$, X-Ray diffraction (XRD), Raman data of $MoS_{2(1-x)}Se_{2x}$ with different x values, catalytic behaviour towards HER with other values of x (x = 0.25, 0.6, 0.75), electrical properties, quantification of XPS data and faradaic efficiency measurements. See DOI: 10.1039/b000000x/

1 Q. H. Wang, K. K. Zadeh, A. Kis, J. N. Coleman, and M. S. Strano, Electronics and optoelectronics of two-dimensional transition metal dichalcogenides, *Nature Nanotech.* 2012, **7**, 699-712.

2 M. Chhowalla, H. S. Shin, G. Eda, L. –J. Li, K. P. Loh, and H. Zhang, The chemistry of two-dimensional layered transition metal dichalcogenide nanosheets, *Nature Chem.* 2013, **5**, 263-275.

3 C. N. R. Rao, H. S. S. R. Matte, and U. Maitra, Graphene Analogues of inorganic layered materials, *Angew. Chem. Int. Ed.* 2013, **52**, 13162-13185.

4 H. S. S. R. Matte, A. Gomathi, A. K. Manna, D. J. Late, R. Datta, S. K. Pati, and C. N. R. Rao, MoS_2 and WS_2 Analogues of graphene, *Angew. Chem. Int. Ed.* 2010, **122**, 4153-4156.

5 H. Wang, Z. Lub, S. Xu, D. Kong, J. J. Cha, G. Zheng, P. –C. Hsu, K. Yan, D. Bradshaw, F. B. Prinz, and Y. Cui, Electrochemical tuning of vertically aligned MoS_2 nanofilms and its application in improving hydrogen evolution reaction, *Proc. Nat. Acad. Sci.* 2013, **110**, 19701-19706.

6 K. –G. Zhou, N. –N. Mao, H. –X. Wang, Y. Peng, and H. –L. Zhang, A mixed-solvent strategy for efficient exfoliation of inorganic graphene analogues, *Angew. Chem. Int. Ed.* 2011, **50**, 10839-10842.

7 G. Cunningham, M. Lotya, C. S. Cucinotta, S. Sanvito, S. D. Bergin, R. Menzel, M. SP. Shaffer, and J. N. Coleman, Solvent exfoliation of transition metal dichalcogenides: Dispersibility of exfoliated nanosheets varies only weakly between compounds, *ACS Nano*, 2012, **6**, 3468–3480.

8 B. Chakraborty, H. S. S. R. Matte, A. K. Sood, and C. N. R. Rao, Layer-dependent resonant Raman scattering of a few layer MoS_2, *J. Raman Spectrosc.* 2013, **44**, 92–96.

9 A. Splendiani, L. Sun, Y. Zhang, T. Li, J. Kim, C. –Y. Chim, G. Galli, and F. Wang, Emerging photoluminescence in monolayer MoS_2, *Nano Lett.*, 2010, **10**, 1271–1275.

10 G. Eda, H. Yamaguchi, D. Voiry, T. Fujita, M. Chen, and M. Chhowalla, Photoluminescence from chemically exfoliated MoS_2, *Nano Lett.*, 2011, **11**, 5111–5116.

11 H. –P. Komsa, and A. V. Krasheninnikov, Electronic structures and optical properties of realistic transition metal dichalcogenide heterostructures from first principles, *Phys. Rev. B*, 2013, **88**, 085318.

12 X. –L. Wei, H. Zhang, G. –C. Guo, X. –B. Li, W. –M. Lau, and L. –M. Liu, Modulating the atomic and electronic structures through alloying and heterostructure of single-layer MoS_2, *J. Mater. Chem. A*, 2014, **2**, 2101-2109.

13 H. Terrones, F. L. Urias, and M. Terrones, Novel hetero-layered materials with tunable direct band gaps by sandwiching different metal disulfides and diselenides, *Scientific Reports*, 2013, **3**, 01549.

14 J. Xi, T. Zhao, D. Wang, and Z. Shuai, Tunable electronic properties of two-dimensional transition metal dichalcogenide alloys: A first-principles prediction, *J. Phys. Chem. Lett.*, 2014, **5**, 285–291.

15 Y. Chen, J. Xi, D. O. Dumcenco, Z. Liu, K. Suenaga, D. Wang, Z. Shuai, Y. –S. Huang, and L. Xie, Tunable band gap photoluminescence from atomically thin transition-metal dichalcogenide alloys, *ACS Nano*, 2013, **7**, 4610-4616.

16 J. Kang, S. Tongay, J. Li, and J. Wu, Monolayer semiconducting transition metal dichalcogenide alloys: Stability and band bowing, *J. App. Phys.*, 2013, **113**, 143703.

17 Y. Gong, Z. Liu, A. R. Lupini, G. Shi, J. Lin, S. Najmaei, Z. Lin, A. L. Elías, A. Berkdemir, G. You, H. Terrones, M. Terrones, R. Vajtai, S. T. Pantelides, S. J. Pennycook, J. Lou, W. Zhou, and P. M. Ajayan, Band gap engineering and layer-by-layer mapping of

selenium-doped molybdenum disulfide *Nano Lett.*, 2014, **14**, 442-449.

18 J. Mann, Q. Ma, P. M. Odenthal, M. Isarraraz, D. Le, E. Preciado, D. Barroso, K. Yamaguchi, G. v. S. Palacio, A. Nguyen, T. Tran, M. Wurch, A. Nguyen, V. Klee, S. Bobek, D. Sun, T. F. Heinz, T. S. Rahman, R. Kawakami, L. Bartels, 2-Dimensional transition metal dichalcogenides with tunable direct band gaps: $MoS_{2(1-x)}Se_{2x}$ Monolayers, *Adv. Mater.*, 2014, **26**, 1399–1404.

19 S. Tongay, D. S. Narang, J. Kang, W. Fan, C. Ko, A. V. Luce, K. X. Wang, J. Suh, K. D. Patel, V. M. Pathak, J. Li, and J. Wu, Two-dimensional semiconductor alloys: Monolayer $Mo_{1-x}W_xSe_2$, *App. Phys. Lett.*, 2014, **104**, 012101.

20 H. Liu, K. K. A. Antwi, S. Chuaa, and D. Chia, Vapor-phase growth and characterization of $Mo_{1-x}W_xS_2$ (0< x<1) atomic layers on 2-inch sapphire substrates, *Nanoscale*, 2014, **6**, 624-629.

21 T. F. Jaramillo, K. P. Jørgensen, J. Bonde, J. H. Nielsen, S. and I. Chorkendorff, Identification of Active Edge Sites for Electrochemical H_2 Evolution from MoS_2 Nanocatalysts, *Science*, 2007, **317**, 100-102.

22 B. Hinnemann, P. G. Moses, J. Bonde, K. P. Jørgensen, J. H. Nielsen, S. Horch, I. Chorkendorff, and J. K. Nørskov, Biomimetic hydrogen evolution: MoS_2 nanoparticles as catalyst for hydrogen evolution, *J. Am. Chem. Soc.*, 2005, **127**, 5308–5309.

23 J. Yang, and H. S. Shin, Recent advances in layered transition metal dichalcogenides for hydrogen evolution reaction, *J. Mater. Chem. A*, 2014, **2**, 5979-5985.

24 D. Kong, J. J. Cha, H. Wang, H. R. Lee, and Y. Cui, First-row transition metal dichalcogenide catalysts for hydrogen evolution reaction, *Energy Environ. Sci.*, 2013, **6**, 3553-3558.

25 H. Tang, K. Dou, C. –C. Kaun, Q. Kuang, S. Yang, $MoSe_2$ nanosheets and their graphene hybrids: synthesis, characterization and hydrogen evolution reaction studies, *J. Mater. Chem. A*, 2014, **2**, 360–364.

26 J. Bonde, P. G. Moses, T. F. Jaramillo, J. K. Nørskov, and I. Chorkendorff, Hydrogen evolution on nano-particulate transition metal sulphides, *Faraday Discuss.*, 2008, **140**, 219–231.

27 S. Sarkar and S. Sampath, Equiatomic ternary chalcogenide: PdPS and its reduced graphene oxide composite for efficient electrocatalytic hydrogen evolution, *Chem.Comm*, 2014, **50**, 7359-7362.

28 D. Kong, H. Wang, J. J. Cha, M. Pasta, K. J. Koski, J. Yao, and Y. Cui, Y. Synthesis of MoS_2 and $MoSe_2$ films with vertically aligned layers, *Nano Lett.*, 2013, **13**, 1341−1347.

29 D. Voiry, H. Yamaguchi, J. Li, R. Silva, D. C. B. Alves, T. Fujita, M. Chen, T. Asefa, V. B. Shenoy, G. Eda, and M. Chhowalla, Enhanced catalytic activity in strained chemically exfoliated WS_2 nanosheets for hydrogen evolution, *Nature Materials*, 2013,**12**, 850–855.

30 D. Voiry, M. Salehi, R. Silva, T. Fujita, M. Chen, T. Asefa, V. B. Shenoy, G. Eda, and M. Chhowalla, Conducting MoS_2 nanosheets as catalysts for hydrogen evolution reaction, *Nano Lett.*, 2013, **13**, 6222−6227.

31 M. A. Lukowski, A. S. Daniel, F. Meng, A. Forticaux, L. Li, and S. Jin, Enhanced hydrogen evolution catalysis from chemically exfoliated metallic MoS_2 nanosheets, *J. Am. Chem. Soc.*, 2013, **135**, 10274−10277.

32 D. J. Li, U. N. Maiti, J. Lim, D. S. Choi, W. J. Lee, Y. Oh, G. Y. Lee, S. O. Kim, Molybdenum sulfide/N-doped CNT forest hybrid catalysts for high-performance hydrogen evolution reaction, *Nano Lett.*, 2014, **14**, 1228−1233.

33 Z. Chen, D. Cummins, B. N. Reinecke, E. Clark, M. K. Sunkara, and T. F. Jaramillo, Core-shell MoO_3-MoS_2 nanowires for hydrogen evolution: A functional design for electrocatalytic materials, *Nano Lett.*, 2011, **11**, 4168–4175.

34 C. Xu, S. Peng, C. Tan, H. Ang, H. Tan, H. Zhang, Q. Yan, Ultrathin S-doped $MoSe_2$ nanosheets for efficient hydrogen evolution, *J. Mater. Chem. A*, 2014, **2**, 5597-5601.

35 D. Merki, H. Vrubel, L. Rovelli, S. Fierro, X. Hu, Fe, Co, and Ni ions promote the catalytic activity of amorphous molybdenum sulfide films for hydrogen evolution, *Chem. Sci.*, 2012, **3**, 2515-2525.

36 W. H. Weber, and R. E. Merlin, *Raman Scattering in Materials Science* , Springer-Verlag , Berlin, **2000**.

37 Y. Liang, L. Zhai, X. Zhao, and D. Xu, Band-gap engineering of semiconductor nanowires through composition modulation**,** *J. Phys. Chem. B*, 2005, **109**, 7120-7123.

38 K. F. Mak, C. Lee, J. Hone, J. Shan and T. F. Heinz, Atomically thin MoS_2: A new direct-gap semiconductor, *Phys. Rev. Lett.*, 2010, **105**, 136805.

39 H. –P. Komsa and A. V. Krasheninnikov, Two-Dimensional Transition Metal Dichalcogenide Alloys: Stability and Electronic Properties, *J. Phys.Chem. Lett.*, 2012, **3**, 3652-3656.

40 D. O. Dumcenco, H. Kobayashi, Z. Liu, Y. –S. Huang, and K. Suenaga, Visualization and quantification of transition metal atomic mixing in $Mo_{1-x}W_xS_2$ single layers, *Nat. Commun.*, 2013, **4**, 1351.

41 J. J. Hu, J. S. Zabinski, J. E. Bultman, J. H. Sanders, and A. A. Voevodin, Structure characterization of pulsed laser deposited MoS_x–WSe_y composite films of tribological interests, *Tribol. Lett.*, 2006, **24**, 127-135.

42 H. Vrubel, D. Merki, and X. Hu, Hydrogen evolution catalyzed by MoS_3 and MoS_2 particles, *Energy Environ. Sci.*, 2012, **5**, 6136-6144.

43 J. R. Mckone, B. F. Sadtler, C. A. Werlang, N. S. Lewis, H. B. Gray, Ni−Mo nanopowders for efficient electrochemical hydrogen evolution, *ACS Catalysis*, 2013, **3**,166-169.

